PNAS RESEARCH ARTICLE | CELL BIOLOGY

Sphingosine kinases regulate ER contacts with late endocytic organelles and cholesterol trafficking

Elisa N. D. Palladino[a], Tytus Bernas[b], Christopher D. Green[a], Cynthia Weigel[a], Sandeep K. Singh[a], Can E. Senkal[a], Andrea Martello[c], John P. Kennelly[d], Erhard Bieberich[e], Peter Tontonoz[d], David A. Ford[f], Sheldon Milstien[a], Emily R. Eden[c], and Sarah Spiegel[a,1]

Edited by Pietro De Camilli, Yale University, New Haven, CT; received March 11, 2022; accepted August 16, 2022

Membrane contact sites (MCS), close membrane apposition between organelles, are platforms for interorganellar transfer of lipids including cholesterol, regulation of lipid homeostasis, and co-ordination of endocytic trafficking. Sphingosine kinases (SphKs), two isoenzymes that phosphorylate sphingosine to the bioactive sphingosine-1-phosphate (S1P), have been implicated in endocytic trafficking. However, the physiological functions of SphKs in regulation of membrane dynamics, lipid trafficking and MCS are not known. Here, we report that deletion of SphKs decreased S1P with concomitant increases in its precursors sphingosine and ceramide, and markedly reduced endoplasmic reticulum (ER) contacts with late endocytic organelles. Expression of enzymatically active SphK1, but not catalytically inactive, rescued the deficit of these MCS. Although free cholesterol accumulated in late endocytic organelles in SphK null cells, surprisingly however, cholesterol transport to the ER was not reduced. Importantly, deletion of SphKs promoted recruitment of the ER-resident cholesterol transfer protein Aster-B (also called GRAMD1B) to the plasma membrane (PM), consistent with higher accessible cholesterol and ceramide at the PM, to facilitate cholesterol transfer from the PM to the ER. In addition, ceramide enhanced in vitro binding of the Aster-B GRAM domain to phosphatidylserine and cholesterol liposomes. Our study revealed a previously unknown role for SphKs and sphingolipid metabolites in governing diverse MCS between the ER network and late endocytic organelles versus the PM to control the movement of cholesterol between distinct cell membranes.

membrane contact sites | sphingolipids | cholesterol | sphingosine kinase | Aster-B/GRAMD1b

Significance

Sphingolipids and cholesterol are important constituents of membranes. Very little is known how their metabolism is cross-regulated and how this affects membrane contact sites (MCS) that control lipid traffic. Here, we report deletion of sphingosine kinases (SphKs) that decreases S1P with concomitant increases in its precursors sphingosine and ceramide, reduced endoplasmic reticulum (ER) contacts with late endocytic organelles leading to accumulation of free cholesterol there. Surprisingly however, cholesterol transport to the ER was not reduced as deletion of SphKs promoted recruitment of cholesterol transfer protein Aster-B to the plasma membrane (PM) to facilitate transfer of cholesterol from the PM to the ER. Thus, SphKs and sphingolipid metabolites govern diverse MCS with the ER to control the movement of cholesterol between distinct cell membranes.

Membrane contact sites (MCS) are highly regulated regions of close membrane apposition between functionally distinct organelles that have emerged as important platforms for nonvesicular interorganellar communication that regulate the dynamic state of cellular compartments as well as control of lipid traffic and homeostasis (1–4). The endocytic pathway brings large amounts of lipids, including cholesterol and sphingolipids, into cells for sorting and degradation in the lysosome. In the past decade, we have begun to appreciate the importance of regulation of interactions between the endoplasmic reticulum (ER) with late endosomes and lysosomes (hereafter referred to as LE/Lys) or with the plasma membrane (PM) at MCS for intracellular lipid transport and distribution that controls the fate of these lipids (2–4).

Efficient transport of endocytosed low-density lipoprotein-derived cholesterol (LDL-cholesterol) from the LE/Lys to the ER, where sterol levels are sensed and cholesterol biosynthesis is regulated, requires Niemann-Pick C (NPC) 1 and NPC2 proteins (5). Structural studies suggested that an NPC1 tunnel bypasses the glycocalyx, which protects the lysosomal membrane from degradative enzymes, to deliver luminal cholesterol from NPC2 to the cytosolic leaflet of the LE/Lys membrane (6). There is also increasing evidence that ER contact sites with late endocytic organelles are conduits for direct LDL-cholesterol transport to the ER by specific sterol binding protein bridges, consisting of endosomal oxysterol-binding protein homolog ORP1L that binds ER-localized vesicle associated membrane protein-associated protein (VAP) (7, 8) and NPC1 that binds ER-resident ORP5 (9). We have previously shown that NPC1 also tethers these MCS where it interacts with the ER-localized sterol transport protein Aster-B (encoded by the *Gramd1b* gene) to regulate cholesterol egress (10). LDL-derived cholesterol can also travel from LE/Lys first to the PM by a process requiring phosphatidylserine (PS) (11) and subsequently to the ER mediated by Aster proteins that bind PS and cholesterol (12–14).

Loss-of-function mutations in NPC1 are major causes of the fatal neurodegenerative lysosomal lipid storage disorder that results in accumulation of unesterified (free) cholesterol and sphingolipids in lysosomes (15–20). However, it is unclear how sphingosine, the final breakdown product of all internalized sphingolipids, also accumulates in

Author contributions: E.N.D.P., E.R.E., and S.S. designed research; E.N.D.P., T.B., C.D.G., C.W., S.K.S., C.E.S., A.M., J.P.K., E.B., P.T., D.A.F., and E.R.E. performed research; E.N.D.P., P.T., D.A.F., S.M., E.R.E., and S.S. analyzed data; and S.M. and S.S. wrote the paper.

The authors declare no competing interest.

This article is a PNAS Direct Submission.

Copyright © 2022 the Author(s). Published by PNAS. This article is distributed under Creative Commons Attribution-NonCommercial-NoDerivatives License 4.0 (CC BY-NC-ND).

[1]To whom correspondence may be addressed. Email: sarah.spiegel@vcuhealth.org.

This article contains supporting information online at http://www.pnas.org/lookup/suppl/doi:10.1073/pnas.2204396119/-/DCSupplemental.

Published September 19, 2022.

Downloaded from https://www.pnas.org by UCL Library Services on September 27, 2022 from IP address 128.41.35.191.

lysosomes (21, 22), and whether NPC1 is also involved in the efflux of sphingosine (23, 24). Nevertheless, sphingolipid metabolism is dependent on egress of sphingosine from lysosomes to reach the machinery required for its reutilization or degradation that is all localized to the ER (25, 26). Sphingosine can be recycled to ceramide by six ER localized ceramide synthases (CerS). Alternatively, it can be phosphorylated by sphingosine kinases (SphK1 and SphK2) to form sphingosine-1-phosphate (S1P) and then irreversibly cleaved by ER localized S1P lyase in the only exit pathway for total sphingolipid degradation (27). Interestingly, SphK1 and SphK2 activities are reduced in NPC1 mutant cells (28–30), suggesting a potential link between SphK activity, NPC1, and cholesterol trafficking and metabolism. Thus, we speculated that conversion of sphingosine to S1P could contribute to the regulation of MCS formation between LE/Lys and the ER. In this regard, despite mounting evidence for cross-regulation of sphingolipids and cholesterol metabolism (31, 32), several key questions remain unanswered, such as how cholesterol and sphingolipid metabolism are coordinated at a mechanistic level, and how this cross-regulation affects MCS and their physiological significance. Here we utilized cells deficient of SphK1, SphK2, or both to begin answering these questions and to investigate their role in regulation of MCS and cholesterol trafficking and metabolism.

Results

Sphingosine Kinases Regulate Lysosomal Positioning. Previous studies showed that SphK1 was recruited to endocytic intermediates (33, 34) and its inhibition impaired endocytic trafficking and caused accumulation of enlarged LE with increased ceramide (34, 35). However, the physiological functions of SphK1 or even SphK2 in regulation of membrane dynamics and lipid trafficking are not known. To this end, SphK1, SphK2, or both were knocked out in HeLa cells using CRISPR/Cas9 genome editing. Western blots confirmed complete absence of SphK1 or SphK2 protein (Fig. 1*A*). As expected, S1P levels were decreased by deleting SphK1 or SphK2 and more dramatically by deletion of both, and concomitant increases in levels of its precursors sphingosine and ceramide with identical results in two different clones from each cell line (Fig. 1*B*). We next examined the effects of these deletions on LE/Lys morphology by LAMP1 immunofluorescence staining and confocal microscopy. Lysosomes were distributed throughout the cytoplasm in control cells, and more clustered in the perinuclear regions in SphK deleted cells with increased LAMP1 staining intensity (Fig. 1 *C*–*E*). In contrast, immunostaining of the ER resident protein calreticulin did not show any obvious differences (Fig. 1*F*). In the course of these studies, we noticed that colocalization of calreticulin with the LE/Lys marker Rab7 quantified by Pearson's correlation coefficient was reduced in SphK-deleted cells (Fig. 1*G*), hinting at a reduction in MCS between the ER and late endocytic organelles.

Deletion of SphKs Reduces ER Contacts with Late Endocytic Organelles. MCS between ER and LE/Lys controls the fate of large amounts of lipids and regulates lipid exchange, protein interactions, and signaling (36, 37). Thus, we used several complementary approaches to examine the involvement of SphKs and sphingolipid metabolites in formation of these MCS. MCS can be examined in situ by the combination of fluorescence lifetime imaging microscopy (FLIM) and Förster resonance energy transfer (FRET). Transfer of energy from an excited donor fluorophore (eGFP) conjugated to LAMP1, that resides primarily across lysosomal membranes, to an acceptor fluorophore (mCherry) conjugated to the ER membrane protein Cb5, the C tail of cytochrome b5, requires the two fluorophores to be within close proximity of 10 nm or less (Fig. 2*A*). As protein proximity increases at MCS, the FRET efficiency increases, causing fluorescence lifetime of the donor (τ, in nanoseconds) to decrease, providing a quantitative measure of the proximity of the two proteins (Fig. 2). Representative cellular distributions of the lifetime are depicted using a pseudocolor scale (Fig. 2*B*). The global τ decrease is illustrated by the shift of GFP fluorescence lifetime distribution (Fig. 2*C*). As expected, a decrease of the LAMP1-GFP mean τ value was detected in control cells expressing both fluorophores compared with cells expressing the donor alone (Fig. 2*C*). FLIM analysis also showed decreased FRET efficiency of the ER/Lys reporter pair proteins with a longer lifetime of the donor in SK2 KO and SK DKO, and in SK1 KO cells to a lesser extent, compared with control cells (Fig. 2 *B*–*D* and *SI Appendix*, Fig. S1), suggesting that deletion of SphKs decreased formation of MCS between ER and Lys.

Limitations of FRET–FLIM measurements are low signal-to-noise ratio and the need for overexpression of tagged proteins that can potentially affect the properties of target organelles. To overcome this, we used the highly sensitive in situ proximity ligation assay (PLA) to examine whether the endogenous ER protein Aster-B and the LE/Lys protein Rab7 were located within 40 nm of each other (Fig. 3 *A* and *B*), which is larger than the size of most MCS (38). Many PLA-positive fluorescent puncta were seen in control cells (Fig. 3 *C* and *D*), but not when either of the primary antibodies was omitted, confirming the specificity of the PLA and indicating the presence of MCS. Significantly fewer puncta were formed in cells knocked out for SphK1, SphK2, or both (Fig. 3 *C* and *D*), indicative of a reduction in the overall number of ER and LE/Lys contacts.

SphK Activity is Required to Maintain ER Contacts with a Subset of Multivesicular Endosomes and Lysosomes. It was of interest to examine whether the reduction of MCS is dependent on SphK activity. Transient expression of GFP-tagged SphK1, but not GFP-tagged catalytically inactive SphK1^{G82D} (ciSphK1-GFP), in SK1 KO cells significantly increased PLA signals compared to expression of GFP control plasmid (Fig. 3*E*). Nevertheless, expression of SphK1-GFP had no effect on MCS formation in CTL cells (Fig. 3*E*). Thus, expression of enzymatically active SphK1-GFP rescued the interactions between ER and LE/Lys in SphK1-deficient cells and indicated that SphK1 can promote MCS dependent on its catalytic activity.

Electron microscopy (EM), the only method with sufficient resolution (< 30 nm) to unequivocally identify ER contacts with electron-dense lysosomes or multivesicular endosomes/bodies (MVBs) that contain discrete intraluminal vesicles, was next utilized (Fig. 4*A*). EM can also distinguish between Epidermal Growth Factor Receptor (EGFR)-containing and non-EGFR–containing MVB subpopulations that are tethered to the ER by distinct protein complexes, by staining EGF-treated cells with an antibody to the EGFR extracellular domain coupled to gold (39–41) (Fig. 4*A*). We found that ER contacts with EGFR-MVBs were unaffected in SK1 KO, SK2 KO, or SK DKO cells, whereas MCS with non-EGFR-MVBs were significantly reduced by 35, 33, and 33% and with lysosomes by 42, 18, and 34%, respectively (Fig. 4*B*). Similar reductions in these MCS were observed when SphKs were down-regulated by specific siRNAs (Fig. 4*E*).

We next performed rescue experiments and determined the effect of SphK1-GFP overexpression on the extent of ER-endocytic

Downloaded from https://www.pnas.org by UCL Library Services on September 27, 2022 from IP address 128.41.35.191.

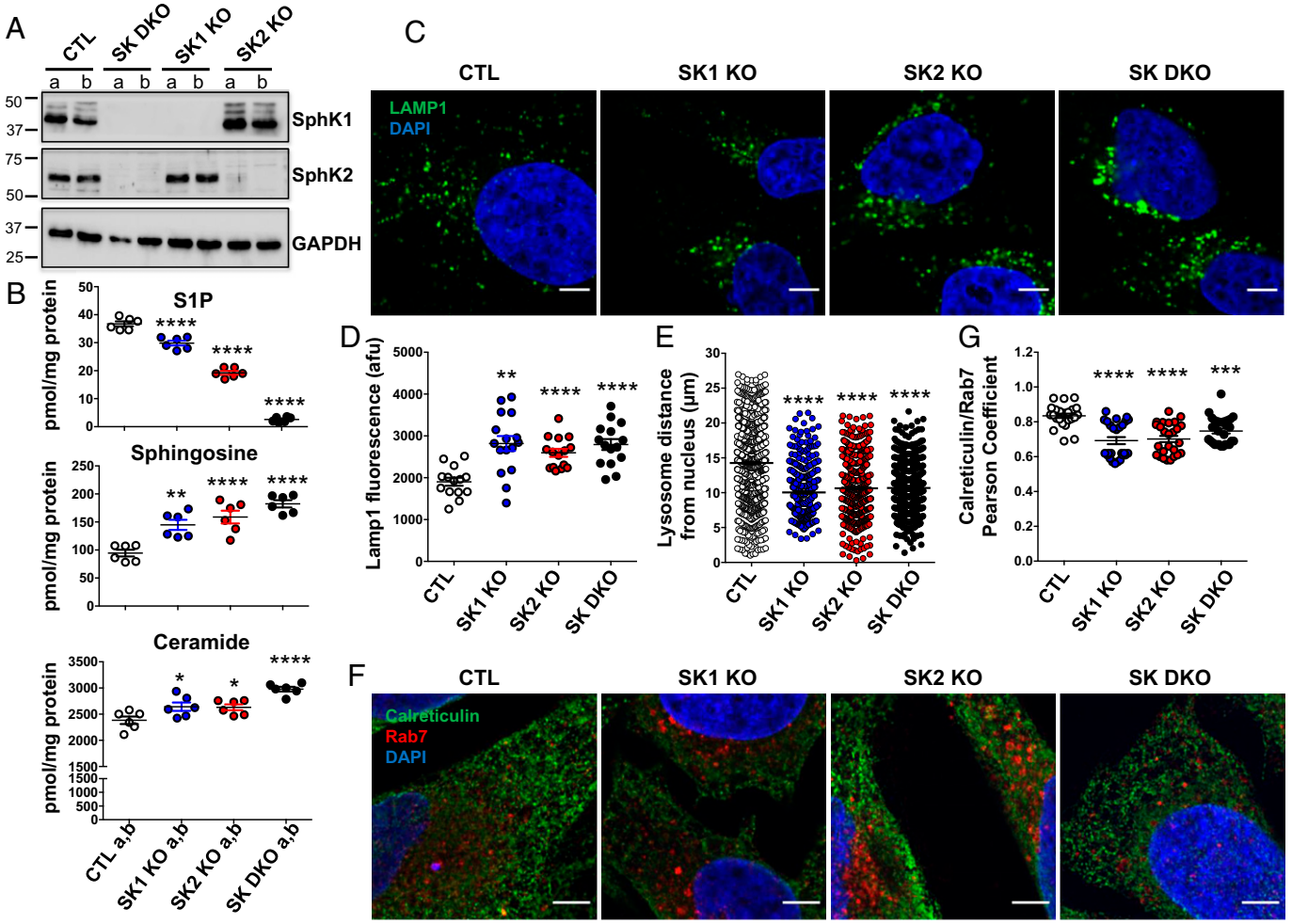

Fig. 1. Deletion of SphK affects lysosomal positioning. (*A*) Expression of SphK1 and SphK2 in HeLa cells with CRISPR/Cas9-mediated deletion of SphK1 (SK1 KO), SphK2 (SK2 KO), or deletion of both (SK DKO) was compared with nontargeted control (CTL) determined by Western blotting. (*B*) Sphingolipids were extracted from the indicated cells and levels of S1P, sphingosine, and total ceramides measured by LC-ESI-MS/MS. *a* and *b* refer to two independent clones. (n = 6). (*C*) Representative confocal images of LAMP1 immunofluorescence staining (green) and nuclei co-stained with DAPI (blue). (Scale bar, 5 μm.) (*D*) LAMP1 fluorescence intensity in the indicated cells expressed as arbitrary fluorescence units (afu). $n \geq 15$ cells from each group. (*E*) The distance of lysosomes from nuclei. n = 3 to 4 cells from each group. Each dot represents a single lysosome. (*F*) Representative confocal images of immunofluorescence staining of Rab7 (red) and calreticulin (green), LE/Lys and ER markers, respectively, and nuclei costained with DAPI (blue). (Scale bar, 5 μm.) (*G*) Quantification of ER and LE/Lys colocalization in the indicated cells by Pearson's correlation coefficients. $n \geq 25$ cells from each group. (*B*, *D*–*G*) Data are mean ± SEM, $^{*}P < 0.05$, $^{**}P < 0.01$, $^{***}P < 0.001$. $^{****}P < 0.0001$ compared to CTL. One-way ANOVA test followed by Dunnett's multiple comparisons test.

organelle MCS in SK1 KO cells. ER contacts with LE/Lys were significantly extended in cells overexpressing SphK1-GFP but not in cells expressing catalytically inactive ciSphK1-GFP (Fig. 4 *C* and *D*), further confirming the requirement for SphK activity for formation of these MCS.

Role of SphK in Cholesterol Transport to the ER. Previous studies reported that MCS between LE/Lys and the ER act as conduits for the transport of LDL-derived cholesterol to the ER (7–10, 42, 43). Since disruption or reduction in these MCS has been implicated in transport blockage of cholesterol delivery to the ER, leading to cholesterol accumulation in LE/Lys (10), we sought to examine the role of SphK in cholesterol egress. Staining with Filipin, a fluorescent dye that specifically binds unesterified cholesterol (44), to visualize cholesterol levels inside the cells revealed intracellular accumulation of cholesterol in SphK-deleted cells (Fig. 5 *A* and *B* and *SI Appendix*, Fig. S2*A*). Indeed, uptake of LDL labeled with BODIPY integrated into the hydrophobic core of LDL was increased in SK DKO cells (*SI Appendix*, Fig. S2*C*). Intracellular cholesterol quantified by the Amplex Red cholesterol assay, confirmed elevated free cholesterol in SphK-deleted cells cultured in Fetal Calf Serum (FCS), which contains LDL (Fig. 5*C*). As a measure of cholesterol transport to the ER, we also quantitated cholesterol ester (CE) levels in these cells, since excess cholesterol is esterified with a fatty acid by the ER-resident acyl-CoA:cholesterol acyltransferase for storage as cholesteryl esters in lipid droplets (5). Surprisingly, CE levels were also significantly increased in these SphK-depleted cells when cultured in the presence of FCS but not in those cultured in lipoprotein-deficient serum (LPDS) (Fig. 5*C*). To confirm these unexpected results, we utilized high-precision mass spectrometry to quantitate CEs. The major saturated and monounsaturated species, CE 16:0 and CE 18:1, respectively, were greatly increased in SK DKO cells cultured in LDL-containing medium compared to CTL (Fig. 5*D*). In addition, neutral lipid droplets visualized with BODIPY493/503 were also increased only in SK DKO cells cultured in FCS (*SI Appendix*, Fig. S2*B*).

When LDL-derived cholesterol released in lysosomes reaches the ER, it also blocks the proteolytic processing and transcriptional activity of the sterol regulatory element-binding protein-2

Downloaded from https://www.pnas.org by UCL Library Services on September 27, 2022 from IP address 128.41.35.191.

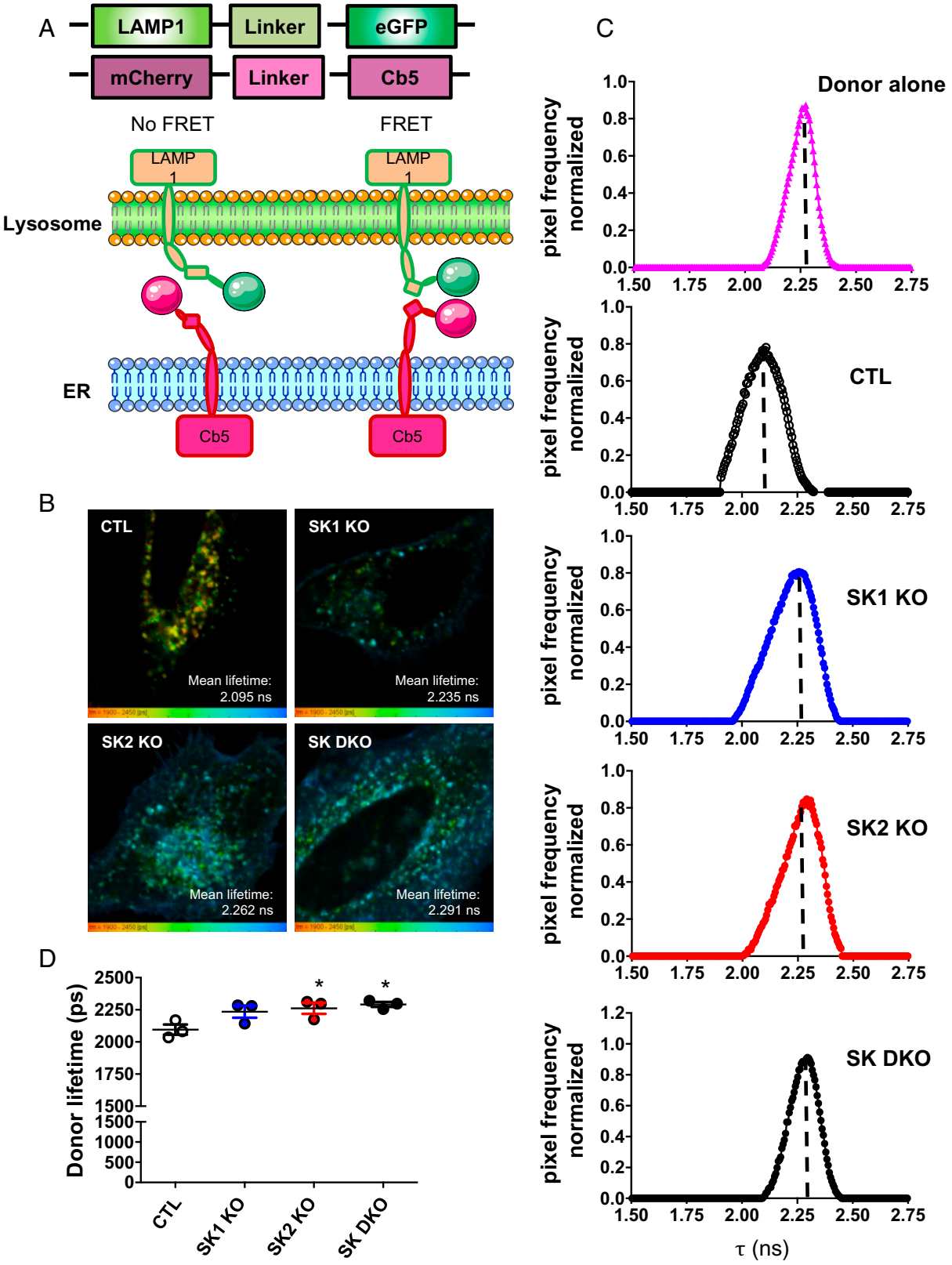

Fig. 2. FRET-FLIM analysis of ER contact sites with late endocytic organelles. (*A*) Schematic representation of the membrane reporter proteins and graphic representation of the topologies of the donor (LAMP1-eGFP) and the acceptor (mCherry-Cb5) fluorophores in the absence or presence of ER-Lys MCS and FRET. (*B*) Cells were transfected with LAMP1-eGFP and mCherry-Cb5 as indicated. Pseudocolor FLIM images show donor (LAMP1-eGFP) mean lifetime (τ) in the presence of the acceptor (mCherry-Cb5) in CTL, SK1 KO, SK2 KO and SK DKO cells. A pseudocolor scale ranging from 1.90 to 2.45 ns represents τ values. (*C*) Distribution of τ values of LAMP1-eGFP (donor) in NTC and DKO cells expressing LAMP1-eGFP and mCherry-Cb5 compared to cells expressing LAMP1-eGFP (donor) only. Data are expressed as normalized pixel frequency. (*D*) Quantification of average donor lifetime in the indicated cells expressing LAMP1-eGFP and mCherry-Cb5. Data are mean ± SD. *$P \leq 0.05$ compared to CTL. One-way ANOVA test followed by Dunnett's multiple comparisons test.

Downloaded from https://www.pnas.org by UCL Library Services on September 27, 2022 from IP address 128.41.35.191.

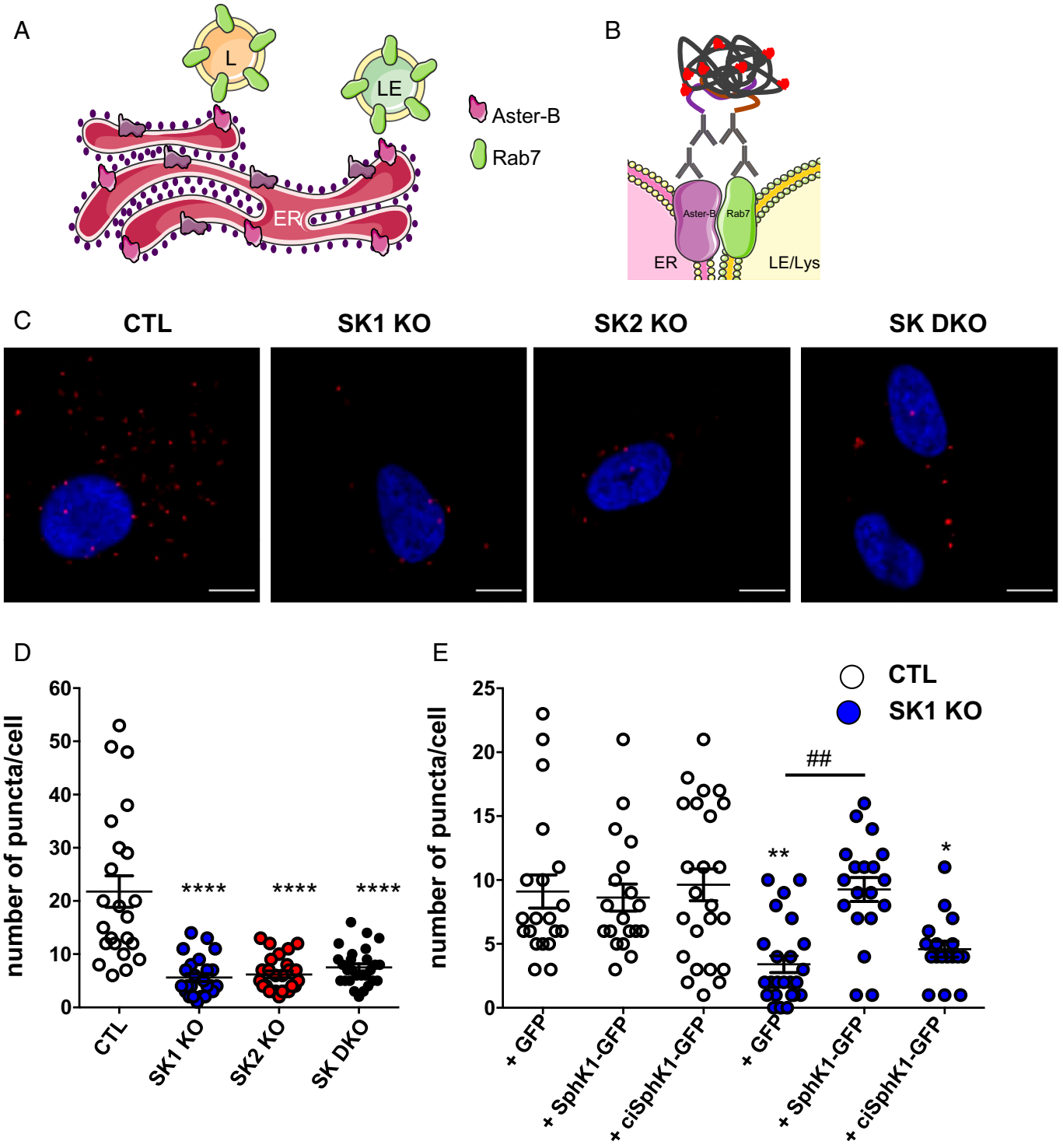

Fig. 3. Effects of SphK deletion on ER contact sites with late endocytic organelles determined by in situ proximity ligation assays. (*A*) Schematic representation of MCS formation between ER and LE/Lys, and (*B*) diagram of PLA. (*C*, *D*) Representative images of the indicated cells labeled with mouse anti-Aster-B and rabbit anti-Rab7 antibodies and subjected to in situ PLA (red) and nuclei stained with DAPI (blue). (Scale bar, 10 μm.) (*D*) Quantification of numbers of PLA puncta per cell. Data are mean ± SEM $n = 24$ to 27 cells from three independent experiments. $^{*}P < 0.05$, one-way ANOVA with Dunnett's test, compared to CTL. (*E*) CTL or SK1 KO cells were transfected with GFP, SphK1-GFP, or GFP-tagged catalytically inactive SphK1^{G82D} (ciSphK1-GFP), and contacts between ER and LE/Lys in transfected cells determined by in situ PLA. Data are the numbers of PLA puncta per cell and are mean ± SEM $n \geq 17$ cells from each group. $^{*}P < 0.05$, $^{***}P < 0.001$. $^{****}P < 0.0001$ compared to CTL. $^{\#\#}P < 0.001$ compared to SK1 KO cells transfected with GFP. One-way ANOVA test followed by Tukey's multiple comparisons test.

(SREBP-2), a master regulator of cholesterol biosynthesis and uptake pathways (5, 45). As expected, incubation of cells with LPDS induced expression of SREBP-2 target genes *HMGCR, HMGCS1,* and *LDLR* (Fig. 5*E*). Only minor changes in the expression of these genes were observed in LPDS-cultured SK DKO cells compared to controls. Taken together, these data suggest that although SphK depletion reduced MCS between ER and late endocytic organelles (Figs. 2–4) with an associated increase in intracellular free cholesterol content (Fig. 5 *A–D*), most cholesterol transport to the ER was not impaired.

Downloaded from https://www.pnas.org by UCL Library Services on September 27, 2022 from IP address 128.41.35.191.

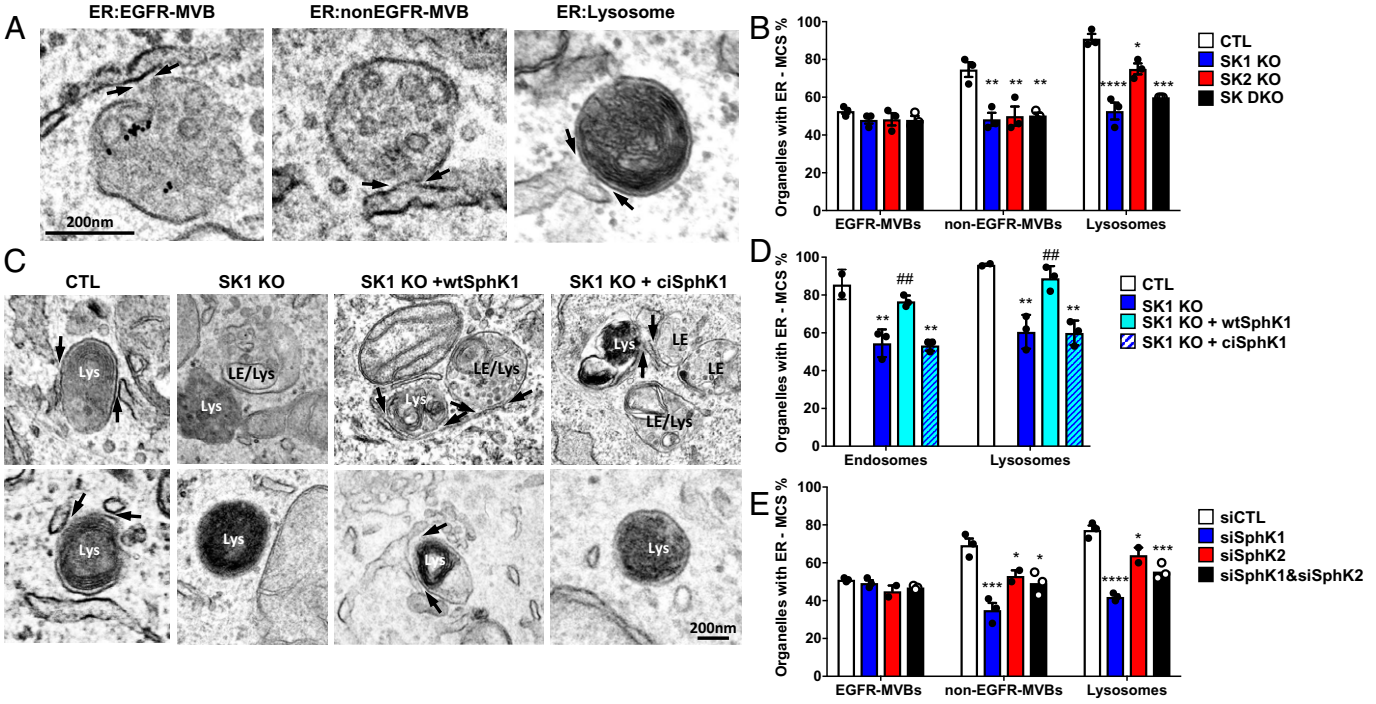

Fig. 4. SphK1 activity is required to maintain MCS between the ER and distinct endocytic organelles. (*A*, *B*) CTL, SK1 KO, SK2 KO, and SK DKO HeLa cells were stimulated with EGF for 45 min in the presence of anti-EGFR coupled to gold prior to EM. (*A*) Representative electron micrographs showing distinct MCS populations. Arrows indicate MCS between the ER and endocytic organelles. (Scale bar, 200 nm.) (*B*) Endocytic organelle populations were scored according to the presence of MCS with the ER and the percentage of organelles with an ER MCS quantified. (*C*, *D*) SK1 KO cells were transfected with SphK1-GFP or ciSphK1-GFP. ER MCS (arrows) with endocytic organelles, example shown in *C*, were quantified in *D*. (Scale bar, 200 nm.) Data are mean ± SD from two or three separate experiments, from analysis of >75 endocytic organelles from 10 cells per experiment. $^{**}P < 0.01$, compared to CTL. $^{\#\#}P < 0.05$ compared to SK1 KO cells. One-way ANOVA test followed by Tukey's multiple comparisons test. (*E*) HeLa cells transfected with nontargeting siRNA (siCTL), siRNA targeting SphK1 (siSphK1), SphK2 (siSphK2), or both (siSphK1 and siSphK2) were stimulated for 30 min with EGF in the presence of anti-EGFR coupled to gold and percentage of organelles with an ER MCS quantified. Data are mean ± SD of three experiments. (*B*, *E*) $^{*}P < 0.05$, $^{**}P < 0.01$, $^{***}P < 0.001$. $^{****}P < 0.0001$ compared to CTL. $^{\#\#}P < 0.05$ compared to SK1 KO cells. One-way ANOVA test followed by Dunnett's multiple comparisons test.

These findings raised an important question: how does cholesterol from late endocytic organelles reach the ER for esterification when MCS between ER and LE/Lys are significantly decreased? Although several studies provided evidence of direct transport of ∼30% of LDL-cholesterol from endosomes to the ER (8, 10, 43), others have shown that LDL-derived cholesterol travels from lysosomes to the PM before moving to the ER (5, 46, 47), thereby safeguarding plasma membrane cholesterol prior to down-regulation of cholesterol production at the ER. To estimate the amount of accessible cholesterol at the PM that can be rapidly transported to the ER, we incubated cells with fluorescently labeled domain 4 of Anthrolysin O (ALOD4), a bacterial cholesterol-binding protein that stains accessible cholesterol at the PM and does not form pores in membranes (47, 48). In line with previous studies (47, 48), treatment of control cells with bacterial sphingomyelinase (SMase) that degrades sphingomyelin (SM) at the PM to ceramide and liberates cholesterol from the SM sequestrated pool, led to increased accessible cholesterol as detected by increased binding of fluorescent ALOD4 at the PM (Fig. 5 *F* and *G*). ALOD4 fluorescence at the PM was also more intense in SK DKO cells compared to control cells only when cultured in the presence of LDL-containing FCS (Fig. 5 *F* and *G*). Together, these data suggest that in SphK-depleted cells, excess cholesterol was still able to reach the PM, increasing the accessible cholesterol pool.

SphK Deletion Promotes Recruitment of Cholesterol Transfer Protein Aster-B to the PM. Previously, we found that the interaction between NPC1 and the ER-localized cholesterol transport protein Aster-B is necessary for cholesterol egress from late endocytic organelles to the ER (10). Others have demonstrated that Aster-B contains a StART-like domain (also called Aster domain) that binds cholesterol and a GRAM domain that can bind anionic lipids such as PS at the PM (12, 13). In the presence of excess metabolically active accessible cholesterol, Aster-B clusters at distinct ER-PM contact sites and transports accessible PM cholesterol to the ER via its StART-like domain (12, 13, 49). Therefore, we sought to check the effects of deletion of SphK on localization of Aster-B. When control cells were cultured in LPDS, Aster-B-GFP displayed a cellular distribution pattern compatible with its ER localization (12, 13, 50) (Fig. 6*A*). As previously reported (13, 50), hydrolysis of SM by treatment with SMase that reduces the sequestration of PM cholesterol and expands the PM accessible cholesterol pool (46), led to recruitment of Aster-B-GFP to the PM (Fig. 6*A*). As expected, SMase treatment also greatly increased ceramide levels (Fig. 6*B*). In this regard, using immunocytochemistry with anti-ceramide antibody (51), we found that the increased ceramide in SK DKO cells is predominantly at the PM and did not colocalize with the lysosome marker LAMP1 (*SI Appendix*, Fig. S3 *A–C*).

Surprisingly, a prominent recruitment of Aster-B-GFP to the PM was also observed in SK DKO cells compared to control cells (Fig. 6 *C* and *E*). Highly inclined thin illumination (HiLo) fluorescence imaging, which allows a higher penetration depth than the Total Internal Reflection Fluorescence (TIRF) mode and has improved signal-to-noise (52), confirmed increased PM localization of Aster-B-GFP in SK DKO cells (Fig. 6*F*). Likewise, immunofluorescence with anti-Aster-B antibody highlighted enhanced staining of endogenous Aster-B at ER tubules that abutted the PM in SphK deleted cells compared to

Downloaded from https://www.pnas.org by UCL Library Services on September 27, 2022 from IP address 128.41.35.191.

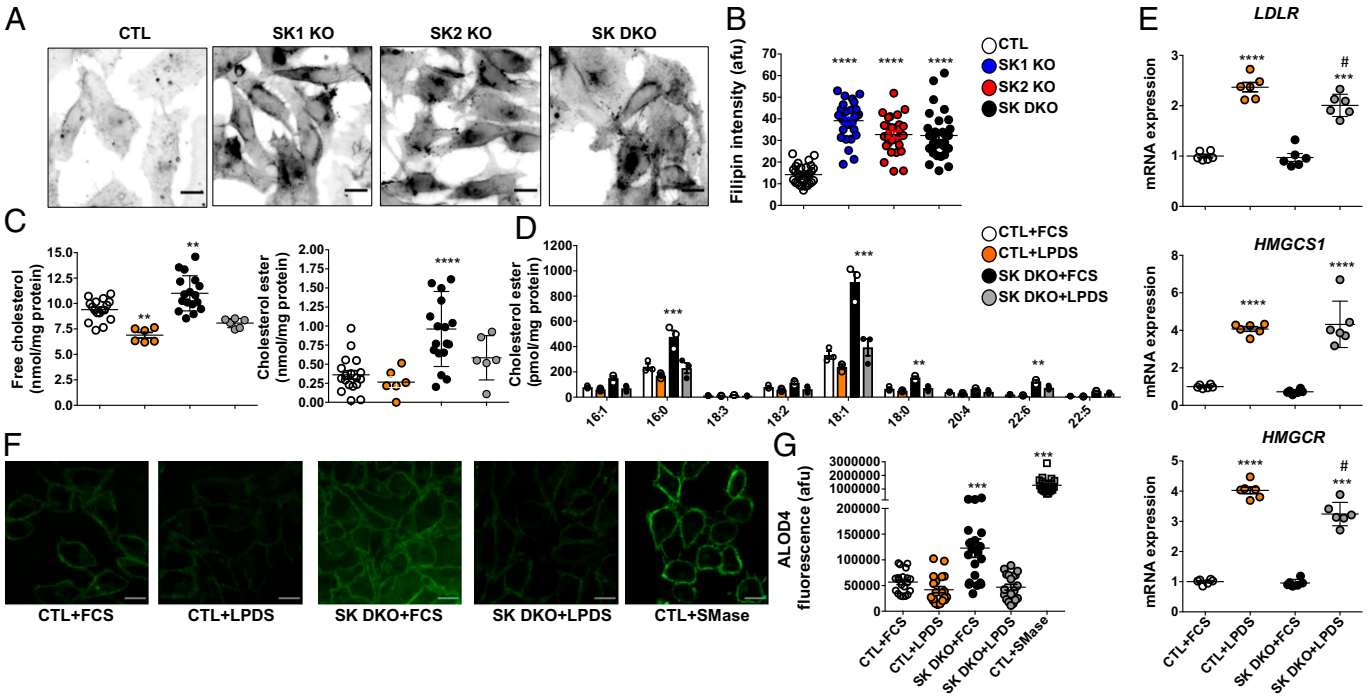

Fig. 5. Effect of SphK deletion on cholesterol transport to the ER. (*A*) Representative confocal microscopy images of CTL, SK1 KO, SK2 KO, and SK DKO HeLa cells cultured in 10% FCS and stained with Filipin (50 μg/mL). (Scale bar, 25 μm.) (*B*) Quantification of Filipin intensity in the indicated cells expressed as arbitrary fluorescence units (afu). $n = 30$ cells from each group. $^{****}P < 0.0001$ compared to CTL. (*C*) Cellular unesterified cholesterol and esterified cholesterol levels in CTL and SK DKO cells cultured in medium containing 5% FCS or LPDS were quantified by Amplex Red assay and are mean ± SEM, $n = 18$, 6 independent cultures from each group. $^{**}P < 0.01$ compared to CTL + FCS. (*D*) ESI-MS/MS analysis of the abundance of cholesterol ester species in CTL and SK DKO cells. Data are mean ± SD ($n = 3$) and are representative of three independent experiments. $^{**}P < 0.01$, $^{***}P < 0.001$ compared to CTL+FCS. (*B–D*) Two-way ANOVA test followed by Dunnett's multiple comparisons test. (*E*) CTL cells (open symbols) and SK DKO cells (closed symbols) were cultured for 24 h in medium containing 5% FCS or LPDS and mRNA expression of genes involved in cholesterol homeostasis determined by QPCR normalized to *GAPDH*. Data are mean ± SEM $n = 6$. $^{***}P < 0.001$, $^{****}P < 0.0001$ compared to cells cultured in FCS. $^{\#}P < 0.05$ compared to CTL cell cultured in LPDS. One-way ANOVA test followed by Tukey's multiple comparisons test. (*F*, *G*) Visualization of PM accessible cholesterol with fluorescent ALOD4 in CTL cells and SK DKO cells cultured for 24 h in medium containing 5% FCS or LPDS. As a positive control, CTL cells were treated with 100 mU/mL sphingomyelinase (SMase) for 30 min. (*G*) Quantification of ALOD4 fluorescence intensity at the PM in the indicated cells expressed as arbitrary fluorescence units (afu). $n = 20$ cells from each group. $^{***}P < 0.001$ compared to CTL + FCS. (*B*, *C*, *E*, *G*) One-way ANOVA test followed by Dunnett's multiple comparisons test.

control cells (Fig. 6 *D* and *E*). Furthermore, we carried out an additional PLA with Aster-B and the phosphatidylethanolamine-binding protein 1 (PEBP1), also known as RAF1 kinase inhibitory protein (RKIP1), which is predominantly localized at the PM (53, 54) (*SI Appendix*, Fig. S4*A*). Significantly higher numbers of PLA puncta were formed in SK DKO cells compared to control cells (*SI Appendix*, Fig. S4 *B* and *C*), confirming that Aster-B was in closer proximity to the PM in SphK depleted cells.

EM was also used to confirm these findings, and in agreement with our previous results (10), revealed that endogenous Aster-B localizes to the ER and at sites of LE/Lys contact (Fig. 7*A*). Importantly, however, there was almost twofold enrichment of the number of gold particles labeling endogenous Aster-B in contact with the PM in cells devoid of SphK compared to control cells (Fig. 7 *A* and *B*). We next analyzed and quantified ER-PM contact zones in control and SphK DKO cells. No accompanying increase in the percentage of PM in contact with ER in SphK DKO compared to control cells was visualized by EM (Fig. 7 *C* and *D*). This finding is consistent with confocal imaging of the ER protein calreticulin, which showed no difference in distribution in the absence of SphK (Fig. 1*F*). Furthermore, as oxysterol binding related proteins 5 (ORP5) has been implicated in lipid transport at ER:PM contact sites (55, 56), we also examined the effect of SphK knockout on ORP5 localization. Expression of ORP5-GFP revealed that in both CTL and SK DKO cells, ORP5 is predominantly expressed in peripheral ER, with no discernable differences in localization between these cell lines (*SI Appendix*, Fig. S5 *A* and *B*). Together, these data suggest that in the absence of SphK, Aster-B is specifically recruited to and enriched at the PM, without expansion of the ER:PM interface.

As Aster-B promotes the movement of cholesterol from the PM to the ER after it leaves the lysosome (12), we next sought to examine the effect of depleting Aster-B on cholesterol transfer to the ER in SK DKO cells. Silencing of Aster-B in SphK depleted cells had no major effects on increased free cholesterol visualized by Filipin staining and quantified by Amplex Red, however it decreased the accumulation of cholesterol esters in these cells (*SI Appendix*, Fig. S6 *A–C*). Similarly, down-regulation of Aster-B also reduced the increase in neutral lipid droplets in SK DKO cells (*SI Appendix*, Fig. S6*D*).

Involvement of Sphingolipid Metabolites in Recruitment of Aster-B to the Plasma Membrane. We began examining the involvement of sphingolipid metabolites regulated by SphKs in PM recruitment of Aster-B. First, overexpression of SphK1 in SphK1-depleted cells not only rescued MCS defects (Fig. 4*D*), it also markedly increased S1P and significantly decreased the elevated levels of several ceramide species (*SI Appendix*, Fig. S7*A*). Moreover, SphK1 overexpression also reduced accumulation of cholesterol esters and the PM recruitment of Aster-B in SphK1-deficient cells (*SI Appendix*, Fig. S7 *B–D*). Second, as S1P actions can be mediated by inside-out signaling and binding to a family of five G protein-coupled receptors, designated S1PR1-5 (57), we considered the possibility that absence of S1PR-mediated effects could be responsible for the observed

Downloaded from https://www.pnas.org by UCL Library Services on September 27, 2022 from IP address 128.41.35.191.

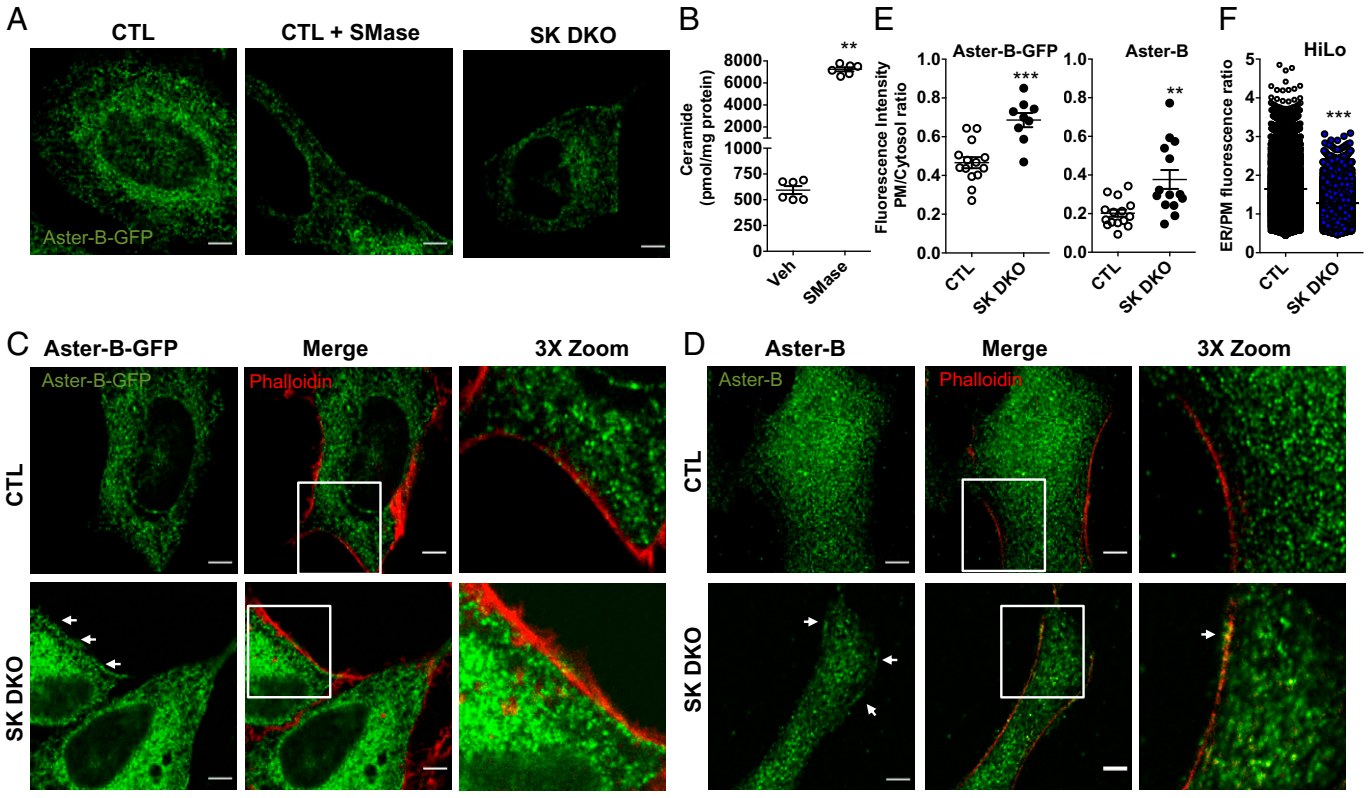

Fig. 6. Aster-B is enriched at ER-PM contact sites in SphK-deficient cells. (*A*) Confocal images of CTL cultured in 5% LPDS treated without or with 100 mU/mL sphingomyelinase (SMase) for 30 min or SK DKO cells expressing Aster-B-GFP as indicated. (*B*) Sphingolipids were extracted from duplicate CTL cells treated without or with SMase and levels of total ceramides measured by LC-ESI-MS/MS. (*C*) Confocal images of CTL and SK DKO cells expressing Aster-B-GFP cultured in 5% FCS. (*D*) Confocal images of CTL and SK DKO cells cultured in 5% FCS and stained with anti-Aster-B antibody. (*E*) Phalloidin staining was used to label edges of the cells to quantify the PM/cytoplasm fluorescence signal intensity ratios for Aster-B-GFP and endogenous Aster-B shown in *C* and *D*, respectively. Arrows indicate ER tubules in close proximity to the PM containing foci of Aster-B expression. (Scale bar, 5 μm.) Data are mean ± SEM $n = 9$ to 14 cells from each group. Results are representative of three independent experiments. (*F*) CTL and SK DKO cells expressing Aster-B-GFP (green), were stained with CellMask Plasma Membrane stain (red). Cells were imaged by the HiLo method and the distribution of pixel fluorescence intensity shown as the ER/PM pixel fluorescence ratio. (*B*, *E*, *F*) $^{**}P < 0.01$, $^{***}P < 0.001$ compared to CTL. Two-tailed unpaired *t* test.

phenotypes. However, treatment of SK DKO with 100 nM S1P, a concentration that activates all the S1P receptors (57), did not reduce accumulation of cholesterol ester (*SI Appendix*, Fig. S8*A*). Nor did it reduce translocation of Aster-B to the plasma membrane (*SI Appendix*, Fig. 8 *B* and *C*), yet, this concentration of S1P activated ERK1/2 in these cells, indicating that the lack of effect is not due to an inability of S1P to signal through its cell surface receptors in SK DKO (*SI Appendix*, Fig. S8*D*). In sharp contrast, decreasing ceramide levels by treatment with Fumonisin B1 (FB1), an inhibitor of ceramide synthases (CerS), reduced the association of Aster-B with the PM in SK DKO cells (*SI Appendix*, Fig. S9 *A* and *B*). Taken together, these data suggest that increased PM ceramide (*SI Appendix*, Fig. S3), and not the absence of S1P receptor-mediated effects, contributes to enhanced Aster-B localization to the PM in SphK depleted cells.

Ceramide Facilitates Interaction of the GRAM Domain with PS and Cholesterol. It has been shown that the phosphatidylserine (PS) binding GRAM domain is both necessary and sufficient for cholesterol-dependent Aster-B recruitment to the PM (12, 13). Thus, it was of interest to explore the possibility that the GRAM domain binds to membranes more efficiently due to the changes in sphingolipids. Because major changes in S1P and its precursors sphingosine and ceramide were observed in SphK null cells, we tested their effects on the binding of the GRAM domain to artificial membranes containing PS in the presence of cholesterol. In this liposome cosedimentation assay, purified GRAM domain of Aster-B was mixed with liposomes containing PS and cholesterol with increasing mole % of sphingolipids. Centrifugation separated GRAM domain bound liposomes in the pellet from the unbound GRAM domain in the supernatant. Consistent with previous findings (58), the GRAM domain of Aster-B bound to liposomes containing 50% cholesterol and 15% PS (Fig. 7*E*). These were selected for further studies as they are similar concentrations to those found in the PM of eukaryotic cells. Intriguingly, incorporation of increasing amounts of the sphingolipid metabolite C16:0 ceramide in these liposomes dose-dependently increased GRAM domain binding to liposomes containing cholesterol and PS (Fig. 7*E*). In contrast, increasing concentrations of sphingomyelin was previously found to decrease binding of the GRAM domain to liposomes (13). Inclusion of sphingosine or S1P in these cholesterol and PS-containing liposomes did not enhance GRAM domain binding, and rather the highest concentration of sphingosine or S1P suppressed binding to the liposomes (Fig. 7*E*). Thus, binding of GRAM domains to membranes that contain cholesterol and PS can be modulated by the presence of specific sphingolipid metabolites. These results support the notion that the recruitment of Aster-B to the PM is regulated by interactions between GRAM domains and PS, and that these interactions can be enhanced by the presence of additional ceramide in the PM.

Discussion

In this study, we have demonstrated an important function for SphKs and the sphingolipid metabolites they regulate in MCS

Downloaded from https://www.pnas.org by UCL Library Services on September 27, 2022 from IP address 128.41.35.191.

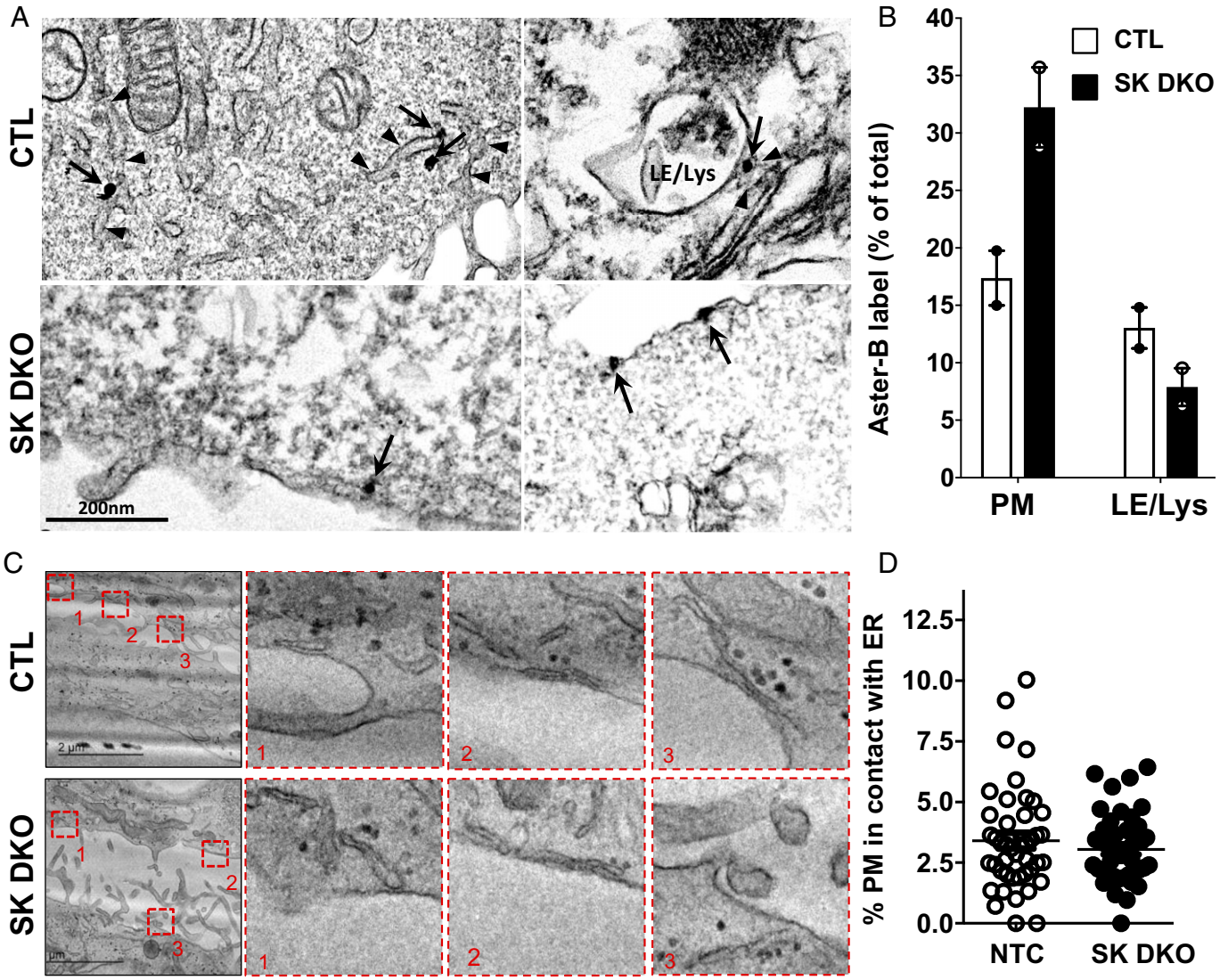

E

C16:0 ceramide

S	P	S	P	S	P	S	P	S	P

Sphingosine

S	P	S	P	S	P	S	P	S	P

S1P

S	P	S	P	S	P	S	P	S	P

PC (mol %)	35	32.5	30	25	20
SL (mol %)	**0**	**2.5**	**5**	**10**	**15**
PS	15	15	15	15	15
Chol (mol %)	50	50	50	50	50

35	32.5	30	25	20
0	**2.5**	**5**	**10**	**15**
15	15	15	15	15
50	50	50	50	50

35	32.5	30	25	20
0	**2.5**	**5**	**10**	**15**
15	15	15	15	15
50	50	50	50	50

Fig. 7. Sphingolipid metabolites affect GRAM domain mediated cholesterol-dependent Aster-B localization. (*A*, *B*) Representative electron micrographs of CTL and SK DKO cells cultured in 5% LPDS and stained with anti-Aster-B antibody and nanogold-secondary antibodies. Arrows indicate endogenous Aster-B staining on the ER (arrowheads), including at ER:LE/Lys contact sites in CTL cells and at the PM in SK DKO cells. (Scale bar, 200 nm.) (*B*) Quantification of the % of Aster-B label within 30 nm of LE/Lys or the PM ($n > 160$ gold particles imaged in two separate experiments/cell type). (*C*) CTL or SK DKO cells were cultured in LPDS for 16 h prior to fixation and preparation for EM. (Scale bar, 2 μm.) (*D*) Quantification of ER-PM contact sites visualized in electron micrographs with 20 cells analyzed per condition in two experiments. Total PM analyzed 439.96 μm and 477.92 μm for CTL and SK DKO, respectively. Data are the percent of PM in contact with the ER and are mean ± SEM $n > 45$ per group. (*E*) Purified GRAM domain of Aster-B was incubated with liposomes containing 35% PC, 50% cholesterol, 15% PS, and increasing mole % of the indicated sphingolipid metabolites, C16:0 ceramide, sphingosine, and S1P in place of PC. Liposomes were sedimented and bound GRAM domain (pellet, P) was separated from unbound GRAM (supernatant, S) and analyzed by immunoblotting for GRAM domain association.

formation between the ER and late endocytic organelles and cholesterol trafficking. Utilizing several complementary approaches including PLA, FRET-FLIM analyses, and EM with higher resolution that allows the contacts themselves to be visualized, we showed that discrete ER-endosome MCS populations are reduced in SphK null cells. While ER contacts with EGFR-containing

Downloaded from https://www.pnas.org by UCL Library Services on September 27, 2022 from IP address 128.41.35.191.

MVBs were unchanged by deletion of SphKs, ER contacts with lysosomes and EGFR-negative MVBs were significantly reduced. Moreover, SphK activity was required to maintain ER contacts with this subset of multivesicular endosomes and the lysosomes. Although recent years have seen major advances in our understanding of ER:endosome MCS (59), the molecular composition of the MCS along the endocytic pathway remains incompletely defined because of their dynamic and transient nature. We previously found that these different populations of endocytic organelles are tethered to the ER by distinct protein complexes (10, 40). EGFR-containing MVBs are tethered by Annexin-A1 and its calcium-dependent ligand S100A11 (40), while several proteins have been implicated in tethering non-EGFR populations, including VAPs (40), NPC1 and Aster-B (10). We have identified a role for SphK, not as a tether itself, but as a regulator of MCS between ER and LE/Lys. How deletion of SphKs so profoundly affects ER contacts with acidic organelles remains unclear, although sphingosine, the final breakdown product of all sphingolipids, can accumulate in the limiting membrane of lysosomes (26). In turn, lysosomal sphingosine accumulation has been implicated in depletion of lysosome calcium stores (21, 23), which have been shown to influence MCS formation between the ER and LE/Lys (39). In addition, it was recently suggested that excessive sphingosine in LE/Lys may compete with cholesterol for NPC1-mediated efflux (24). If Aster-B favors interaction with sterol-bound NPC1 as proposed (10), sphingosine accumulation could also reduce NPC1-tethered MCS but effects on other NPC1-independent MCS cannot be excluded.

Similar reductions in ER contacts with lysosomes and non-EGFR-MVBs were seen in NPC1-deficient cells (10). We now show that diminished numbers of MCS between the ER and endocytic organelles lead to cholesterol accumulation in LE/Lys that also characterizes NPC1-deficient cells. Our results also support an important function for these MCS in direct transport of LDL-cholesterol from endocytic organelles to the ER and are consistent with previous reports that expansion of LE/Lys and ER MCS can reduce cholesterol accumulation in NPC1 mutant or deficient cells (10, 60). Like NPC1-deficient cells, LE/Lys also clustered in the perinuclear region of SphK-deleted cells. This may be due to accumulation of cholesterol that affects LE/Lys traffic and localization (37) by conformational change of the cholesterol-sensing protein ORP1L (7). The reduction in peripheral LE/Lys in SphK KO cells may impact their accessibility for interactions with tubular ER, but is also likely to be, at in least in part, a consequence of reduced ER contact since ER:LE/Lys MCS have been implicated in governing endosome positioning (2, 3).

Similar to NPC1-deficient cells (15, 16, 20, 61), although to a lesser extent, unesterified, cholesterol accumulated in endocytic organelles in the absence of SphKs. However, in striking contrast to reduced cholesterol esterification in NPC1-depleted cells (10), cholesterol ester levels in SphK null cells were increased. These results indicate that LDL-derived cholesterol was able to reach the ER despite a reduction in MCS between LE/Lys and ER and that the ER is not starved of cholesterol in the absence of SphKs. Instead, LDL-derived cholesterol trafficked to the ER, at least in part from the PM. Once at the ER, cholesterol is esterified with a fatty acid for storage as CE in lipid droplets and blocks SREBP-2 activation to turn off transcription of genes for cholesterol synthesis and uptake (5). Our data also suggest that in contrast to NPC1, which is required for cholesterol egress from endocytic organelles, SphK activity is dispensable for LE/Lys cholesterol transport to the PM and then to the ER.

Intriguingly, we found that deletion of SphKs promoted PM recruitment of Aster-B that facilitates movement of the accessible pool of cholesterol from the PM to ER (12–14, 49). Once levels of cholesterol in the PM rise above a threshold, Aster-B forms bridges between the PM to the ER, and its StART-like domain extracts accessible cholesterol from the PM and transfers it to the ER down the concentration gradient (12, 13, 49). Binding of its GRAM domain to PS, a major acidic phospholipid in the inner leaflet of PM, is heightened by excess cholesterol (12). We found that these interactions are intensely enhanced by ceramide that increases at the PM in SphK-deleted cells. Our data support the notion that in SphK-depleted cells, excess LDL-derived cholesterol trafficked to the PM increases the accessible cholesterol pool (as revealed by increased binding of ALOD4), which is the only pool free to move to the ER (46–48). We can also speculate that the presence of an elevated level of ceramide may reduce the concentration threshold for accessible cholesterol and PS in the PM bilayer to facilitate the localization of Aster-B at PM-ER contacts and enhance transport of cholesterol. It is important to note that previous studies have shown that sphingomyelin suppresses binding of the GRAM domain to model membranes that contain cholesterol and PS and conversely, treatment with sphingomyelinase stimulates Aster-B translocation to the PM (13, 50). It was suggested that sphingomyelinase liberates the sphingomyelin-sequestered pool of PM cholesterol into the accessible pool that can then be transported by Aster-B to the ER (13, 50). Our data provide an additional explanation for this effect as sphingomyelinase degrades sphingomyelin and produces large amounts of ceramide at the PM that in turn can augment Aster-B-mediated transport of PM cholesterol to the ER.

We previously reported that Aster-B also interacts with NPC1 at ER-lysosome contact sites in the presence of high LDL-cholesterol in the endocytic pathway for cholesterol transport to the ER (10). We suggested that both NPC1 and Aster-B have dual roles in transport of LDL-derived cholesterol to the ER (62), participating in direct ER-lysosome contact sites and in indirect transport from lysosomes to the PM before moving to the ER (10). Remarkably, deletion of SphKs and changes in sphingolipids, while reducing MCS between LE/Lys and the ER, enhances the indirect pathway by promoting targeting of Aster-B to ER-PM contact sites, likely due to increased PM accessible cholesterol and ceramide, to facilitate transfer of cholesterol from the PM to the ER. Taken together, our study revealed a previously unknown role for SphKs and changes in bioactive sphingolipid metabolites in governing regulation of diverse MCS between the ER network and late endocytic organelles versus the PM to control the movement of cholesterol between distinct cell membranes. Hence, sphingolipid metabolites are emerging as additional players in membrane dynamics and cholesterol trafficking, highlighting the importance of the lipid environment in regulating MCS formation and function.

Despite the growing evidence for cross-regulation of sphingolipids and cholesterol, the dynamic relationship between these lipids has remained elusive. Our studies showed that SphK-mediated changes in sphingolipid metabolites regulate how the ER communicates with the PM and acidic organelles to monitor and respond to changes in cholesterol content. It also demonstrates that a change in sphingolipid metabolites controls the movement of another lipid—cholesterol—between organelles. We believe that this helps to answer the long-sought question of how cholesterol homeostasis is closely coregulated with that of sphingolipid metabolism (31). It also provides

Downloaded from https://www.pnas.org by UCL Library Services on September 27, 2022 from IP address 128.41.35.191.

deeper understanding of how perturbations of sphingolipid metabolism contribute to MCS dysfunctions that are associated with a number of human diseases (36).

Materials and Methods

Generation of SphK knockout HeLa cells by CRISPR/Cas9, cell culture and transfections, plasmids, antibodies, Western blotting, electron microscopy quantitation and immuno-EM, fluorescence imaging and analysis, FRET-FLIM, PLA, lipid analyses, liposome binding assays, QPCR, and statistical analyses are described in detail in *SI Appendix, Materials and Methods*.

Data, Materials, and Software Availability. All study data are included in the article and/or supporting information.

ACKNOWLEDGMENTS. This work was supported by NIH grant R01GM043880 (S.S.). The authors acknowledge the Virginia Commonwealth University Lipidomics/Metabolomics and the Microscopy Shared resources, which are supported in part by funding from the NIH-NCI Cancer Center Support Grant P30 CA016059. A.M. was supported by the Medical Research Council grant MR/V013882/1. Cholesterol ester measurements were supported by NIH grant S10OD025246 (D.A.F.). E.B. was supported by VA grant I01BX003643. We are grateful for the generous gifts from Dr. Maria Antonietta De Matteis (University of Naples) for plasmids; Dr. Arun Radhakrishnan (UT Southwestern) for ALOD4.

Author affiliations: [a]Department of Biochemistry and Molecular Biology, Virginia Commonwealth University School of Medicine, Richmond, VA 23298; [b]Department of Anatomy and Neurobiology, Virginia Commonwealth University School of Medicine, Richmond, VA 23298; [c]UCL Institute of Ophthalmology, London EC1V 9EL, United Kingdom; [d]Department of Pathology and Laboratory Medicine, University of California, Los Angeles, CA 90095; [e]Department of Physiology, University of Kentucky and Veteran Affairs Medical Center, Lexington, KY 40536; and [f]Edward A. Doisy Department of Biochemistry and Molecular Biology, and Center for Cardiovascular Research, Saint Louis University School of Medicine, St. Louis, MO 63104

1. R. van der Kant, J. Neefjes, Small regulators, major consequences–Ca^{2+} and cholesterol at the endosome-ER interface. *J. Cell Sci.* **127**, 929–938 (2014).
2. M. J. Phillips, G. K. Voeltz, Structure and function of ER membrane contact sites with other organelles. *Nat. Rev. Mol. Cell Biol.* **17**, 69–82 (2016).
3. E. R. Eden, The formation and function of ER-endosome membrane contact sites. *Biochim. Biophys. Acta* **1861** (8 Pt B), 874–879 (2016).
4. S. Muallem, W. Y. Chung, A. Jha, M. Ahuja, Lipids at membrane contact sites: Cell signaling and ion transport. *EMBO Rep.* **18**, 1893–1904 (2017).
5. J. L. Goldstein, M. S. Brown, A century of cholesterol and coronaries: From plaques to genes to statins. *Cell* **161**, 161–172 (2015).
6. M. B. L. Winkler *et al.*, Structural insight into eukaryotic sterol transport through Niemann-Pick Type C proteins. *Cell* **179**, 485–497.e18 (2019).
7. N. Rocha *et al.*, Cholesterol sensor ORP1L contacts the ER protein VAP to control Rab7-RILP-p150 Glued and late endosome positioning. *J. Cell Biol.* **185**, 1209–1225 (2009).
8. K. Zhao, N. D. Ridgway, Oxysterol-binding protein-related protein 1L regulates cholesterol egress from the endo-lysosomal system. *Cell Rep.* **19**, 1807–1818 (2017).
9. X. Du *et al.*, A role for oxysterol-binding protein-related protein 5 in endosomal cholesterol trafficking. *J. Cell Biol.* **192**, 121–135 (2011).
10. D. Höglinger *et al.*, NPC1 regulates ER contacts with endocytic organelles to mediate cholesterol egress. *Nat. Commun.* **10**, 4276–4290 (2019).
11. M. N. Trinh *et al.*, Last step in the path of LDL cholesterol from lysosome to plasma membrane to ER is governed by phosphatidylserine. *Proc. Natl. Acad. Sci. U.S.A.* **117**, 18521–18529 (2020).
12. J. Sandhu *et al.*, Aster proteins facilitate nonvesicular plasma membrane to ER cholesterol transport in mammalian cells. *Cell* **175**, 514–529.e20 (2018).
13. T. Naito *et al.*, Movement of accessible plasma membrane cholesterol by the GRAMD1 lipid transfer protein complex. *eLife* **8**, e51401 (2019).
14. M. N. Trinh *et al.*, Interplay between Asters/GRAMD1s and phosphatidylserine in intermembrane transport of LDL cholesterol. *Proc. Natl. Acad. Sci. U.S.A.* **119**, e2120411119 (2022).
15. E. D. Carstea *et al.*, Niemann-Pick C1 disease gene: Homology to mediators of cholesterol homeostasis. *Science* **277**, 228–231 (1997).
16. S. K. Loftus *et al.*, Murine model of Niemann-Pick C disease: Mutation in a cholesterol homeostasis gene. *Science* **277**, 232–235 (1997).
17. E. B. Neufeld *et al.*, The Niemann-Pick C1 protein resides in a vesicular compartment linked to retrograde transport of multiple lysosomal cargo. *J. Biol. Chem.* **274**, 9627–9635 (1999).
18. P. G. Pentchev, Niemann-Pick C research from mouse to gene. *Biochim. Biophys. Acta* **1685**, 3–7 (2004).
19. M. T. Vanier, Niemann-Pick diseases. *Handb. Clin. Neurol.* **113**, 1717–1721 (2013).
20. M. T. Vanier, Complex lipid trafficking in Niemann-Pick disease type C. *J. Inherit. Metab. Dis.* **38**, 187–199 (2015).
21. E. Lloyd-Evans *et al.*, Niemann-Pick disease type C1 is a sphingosine storage disease that causes deregulation of lysosomal calcium. *Nat. Med.* **14**, 1247–1255 (2008).
22. A. K. Tharkeshwar *et al.*, A novel approach to analyze lysosomal dysfunctions through subcellular proteomics and lipidomics: The case of NPC1 deficiency. *Sci. Rep.* **7**, 41408 (2017).
23. D. Höglinger *et al.*, Intracellular sphingosine releases calcium from lysosomes. *eLife* **4**, e10616 (2015).
24. J. Altuzar *et al.*, Lysosome-targeted lipid probes reveal sterol transporters NPC1 and LIMP-2 as sphingosine transporters. https://www.biorxiv.org/content/10.1101/2021.11.10.468010v1.full (2022).
25. S. Spiegel, S. Milstien, Sphingosine-1-phosphate: An enigmatic signalling lipid. *Nat. Rev. Mol. Cell Biol.* **4**, 397–407 (2003).
26. Y. A. Hannun, L. M. Obeid, Sphingolipids and their metabolism in physiology and disease. *Nat. Rev. Mol. Cell Biol.* **19**, 175–191 (2018).
27. M. Maceyka, S. Spiegel, Sphingolipid metabolites in inflammatory disease. *Nature* **510**, 58–67 (2014).
28. H. Lee *et al.*, Pathological roles of the VEGF/SphK pathway in Niemann-Pick type C neurons. *Nat. Commun.* **5**, 5514 (2014).
29. J. Newton *et al.*, Targeting defective sphingosine kinase 1 in Niemann-Pick type C disease with an activator mitigates cholesterol accumulation. *J. Biol. Chem.* **295**, 9121–9133 (2020).
30. M. Lei *et al.*, Sphingosine kinase 2 potentiates amyloid deposition but protects against hippocampal volume loss and demyelination in a mouse model of Alzheimer's disease. *J. Neurosci.* **39**, 9645–9659 (2019).
31. D. K. Breslow, J. S. Weissman, Membranes in balance: Mechanisms of sphingolipid homeostasis. *Mol. Cell* **40**, 267–279 (2010).
32. J. T. Hannich, K. Umebayashi, H. Riezman, Distribution and functions of sterols and sphingolipids. *Cold Spring Harb. Perspect. Biol.* **3**, a004762 (2011).
33. H. Shen *et al.*, Coupling between endocytosis and sphingosine kinase 1 recruitment. *Nat. Cell Biol.* **16**, 652–662 (2014).
34. S. Lima, S. Milstien, S. Spiegel, Sphingosine and Sphingosine Kinase 1 involvement in endocytic membrane trafficking. *J. Biol. Chem.* **292**, 3074–3088 (2017).
35. M. M. Young *et al.*, Sphingosine Kinase 1 cooperates with autophagy to maintain endocytic membrane trafficking. *Cell Rep.* **17**, 1532–1545 (2016).
36. W. A. Prinz, A. Toulmay, T. Balla, The functional universe of membrane contact sites. *Nat. Rev. Mol. Cell Biol.* **21**, 7–24 (2020).
37. A. Martello, F. M. Platt, E. R. Eden, Staying in touch with the endocytic network: The importance of contacts for cholesterol transport. *Traffic* **21**, 354–363 (2020).
38. L. Scorrano *et al.*, Coming together to define membrane contact sites. *Nat. Commun.* **10**, 1287 (2019).
39. B. S. Kilpatrick *et al.*, An endosomal NAADP-sensitive two-pore Ca^{2+} channel regulates ER-endosome membrane contact sites to control growth factor signaling. *Cell Rep.* **18**, 1636–1645 (2017).
40. E. R. Eden *et al.*, Annexin A1 tethers membrane contact sites that mediate ER to endosome cholesterol transport. *Dev. Cell* **37**, 473–483 (2016).
41. J. R. Edgar, E. R. Eden, C. E. Futter, Hrs- and CD63-dependent competing mechanisms make different sized endosomal intraluminal vesicles. *Traffic* **15**, 197–211 (2014).
42. K. W. Underwood, N. L. Jacobs, A. Howley, L. Liscum, Evidence for a cholesterol transport pathway from lysosomes to endoplasmic reticulum that is independent of the plasma membrane. *J. Biol. Chem.* **273**, 4266–4274 (1998).
43. S. Heybrock *et al.*, Lysosomal integral membrane protein-2 (LIMP-2/SCARB2) is involved in lysosomal cholesterol export. *Nat. Commun.* **10**, 3521 (2019).
44. M. T. Vanier, P. Latour, Laboratory diagnosis of Niemann-Pick disease type C: The filipin staining test. *Methods Cell Biol.* **126**, 357–375 (2015).
45. M. S. Brown, J. L. Goldstein, The SREBP pathway: Regulation of cholesterol metabolism by proteolysis of a membrane-bound transcription factor. *Cell* **89**, 331–340 (1997).
46. A. Das, M. S. Brown, D. D. Anderson, J. L. Goldstein, A. Radhakrishnan, Three pools of plasma membrane cholesterol and their relation to cholesterol homeostasis. *eLife* **3**, e02882 (2014).
47. R. E. Infante, A. Radhakrishnan, Continuous transport of a small fraction of plasma membrane cholesterol to endoplasmic reticulum regulates total cellular cholesterol. *eLife* **6**, e25466 (2017).
48. K. A. Johnson, S. Endapally, D. C. Vazquez, R. E. Infante, A. Radhakrishnan, Ostreolysin A and anthrolysin O use different mechanisms to control movement of cholesterol from the plasma membrane to the endoplasmic reticulum. *J. Biol. Chem.* **294**, 17289–17300 (2019).
49. M. Besprozvannaya *et al.*, GRAM domain proteins specialize functionally distinct ER-PM contact sites in human cells. *eLife* **7**, e31019 (2018).
50. B. Ercan, T. Naito, D. H. Z. Koh, D. Dharmawan, Y. Saheki, Molecular basis of accessible plasma membrane cholesterol recognition by the GRAM domain of GRAMD1b. *EMBO J.* **40**, e106524 (2021).
51. K. Krishnamurthy, S. Dasgupta, E. Bieberich, Development and characterization of a novel anti-ceramide antibody. *J. Lipid Res.* **48**, 968–975 (2007).
52. M. Tokunaga, N. Imamoto, K. Sakata-Sogawa, Highly inclined thin illumination enables clear single-molecule imaging in cells. *Nat. Methods* **5**, 159–161 (2008).
53. A. E. Granovsky *et al.*, Raf kinase inhibitory protein function is regulated via a flexible pocket and novel phosphorylation-dependent mechanism. *Mol. Cell. Biol.* **29**, 1306–1320 (2009).
54. S. E. Wenzel *et al.*, PEBP1 wardens ferroptosis by enabling lipoxygenase generation of lipid death signals. *Cell* **171**, 628–641.e26 (2017).
55. J. Chung *et al.*, INTRACELLULAR TRANSPORT. PI4P/phosphatidylserine countertransport at ORP5- and ORP8-mediated ER-plasma membrane contacts. *Science* **349**, 428–432 (2015).
56. R. Ghai *et al.*, ORP5 and ORP8 bind phosphatidylinositol-4, 5-biphosphate ($PtdIns(4,5)P_2$) and regulate its level at the plasma membrane. *Nat. Commun.* **8**, 757 (2017).
57. G. T. Kunkel, M. Maceyka, S. Milstien, S. Spiegel, Targeting the sphingosine-1-phosphate axis in cancer, inflammation and beyond. *Nat. Rev. Drug Discov.* **12**, 688–702 (2013).
58. A. Ferrari *et al.*, Aster proteins regulate the accessible cholesterol pool in the plasma membrane. *Mol. Cell. Biol.* **40**, e00255-20 (2020).
59. S. Jean, S. Nassari, Regulation of endosomal sorting and maturation by ER-endosome contact sites. *Contact (Thousand Oaks)* **5**, 1–9 (2022).
60. E. Meneses-Salas *et al.*, Annexin A6 modulates TBC1D15/Rab7/StARD3 axis to control endosomal cholesterol export in NPC1 cells. *Cell. Mol. Life Sci.* **77**, 2839–2857 (2020).
61. X. Xie *et al.*, Amino acid substitution in NPC1 that abolishes cholesterol binding reproduces phenotype of complete NPC1 deficiency in mice. *Proc. Natl. Acad. Sci. U.S.A.* **108**, 15330–15335 (2011).
62. S. G. Pfisterer, J. Peränen, E. Ikonen, LDL-cholesterol transport to the endoplasmic reticulum: Current concepts. *Curr. Opin. Lipidol.* **27**, 282–287 (2016).

Downloaded from https://www.pnas.org by UCL Library Services on September 27, 2022 from IP address 128.41.35.191.